Trapping effects in HgCdTe

Y. Nemirovsky, R. Fastow, M. Meyassed, and A. Unikovsky
Kidron Microelectronics Research Center, Department of Electrical Engineering, Technion-Israel Institute of Technology, Haifa 32000, Israel

(Received 2 October 1990; accepted 4 December 1990)

Carrier trapping influences the performance of HgCdTe infrared detectors in the 8–12 μm range by enhancing tunneling currents, reducing excess carrier lifetimes, and increasing g–r and $1/f$ noise. In this work, the effects of carrier trapping on the tunneling currents in n^+p diodes are calculated, and the dependence of the tunneling current on temperature, bias, doping level, and trap characteristics is illustrated. It is shown that by assuming the dominant trap energy to be at the Fermi level, the calculated tunneling currents exhibit many of the peculiar features which have been observed experimentally. The related effects that minority carrier traps have on the excess carrier lifetimes are also discussed, and a simple method of estimating many of the relevant trapping characteristics from lifetime measurements is presented.

I. INTRODUCTION

Understanding the dynamics of trapping and the properties of traps in HgCdTe is required for characterizing material grown by various methods and obtained from different sources. The presence of traps affects the performance of all HgCdTe detectors regardless of their type or configuration.

In the past two decades, different techniques have been applied to identify traps and to determine their energy distribution and density, such as deep level transient spectroscopy (DLTS),[1,2] diode pulse recovery,[3,4] optical modulation absorption (OMA), and more recently the two-photon magneto-optical (TPMO) technique.[5] In addition, a number of theoretical approaches have been applied to estimate the properties of defects and traps in HgCdTe.[6–9]

This paper focuses on trapping phenomena that is directly related and extracted from current HgCdTe detectors [i.e. photoconductors and metal-insulator semiconductors (MIS) as well as junction photodiodes].

Three topics are considered:

(a) Trap-assisted tunneling in MIS and junction photodiodes.

(b) Trapping and recombination processes, as related to the excess carrier lifetime in steady state and transient measurements.

(c) Trapping as related to the noise current spectral density of devices.

A. Trap-assisted tunneling

At operating temperatures ~77 K, trap-assisted tunneling is the dominant dark current mechanism over a wide range of biases in long-wavelength infrared LWIR HgCdTe MIS diodes[10–12] as well as in junction photodiodes.[13–22] Trap-assisted tunneling exhibits a distinct temperature dependence that is remarkably different from band-to-band tunneling or thermally limited mechanisms.

In this study, we model the bias dependence as well as the temperature dependence of trap-assisted tunneling. The model is based on two assumptions: that the dominant energy level in trap-assisted tunneling coincides with the Fermi level, and that the tunneling proceeds via thermally excited bulk Shockley-Read centers. Hence, we term this mechanism as thermal-trap-assisted tunneling. The model presented in this study qualitatively fits previously measured data for MIS diodes and junction photodiodes fabricated on p-type material. It should be noted that the process of surface recombination is not included.

B. Trapping and the excess carrier lifetime

Trapping is responsible for the large variation in reported "lifetimes" in p-type material. In particular, in material dominated by Shockley-Read recombination, trapping is manifested by the large differences between steady state "lifetimes" and transient "lifetimes" measured on the same samples.[23–26] A simple approach is presented which illuminates the role of trapping in lifetime experiments and correlates the transient and steady state "lifetimes" with the properties of the trapping centers.

C. Trapping and noise

Traps contribute two types of excess noise in devices: $1/f$ noise which is correlated with the dark current associated with trap-assisted tunneling, and generation-recombination noise.[27] The noise current spectral density can be modeled with the two types of tunneling currents. However, this topic is beyond the scope of the current paper and it will be reported elsewhere.

II. THERMAL-TRAP-ASSISTED TUNNELING IN HgCdTe MIS AND JUNCTION PHOTODIODES

Thermal-trap-assisted tunneling is the dominant dark current mechanism for HgCdTe MIS and junction photodiodes, over a wide range of operating temperatures and voltages. By modeling thermal-trap-assisted tunneling, trapping effects in HgCdTe can be quantitatively analyzed.

Tunneling is often a dominant current mechanism in HgCdTe photodiodes due to the narrow band gap of $x \cong 0.22$ material (~0.1 eV at 77 K), the small effective mass of

 0734-211X/91/031829-11$01.00

electrons in HgCdTe ($m_e^*/M_0 = 7\times10^{-2}E_g$), and the cryogenic temperatures of its operation.

De Wames *et al.*,[13-15] Kinch *et al.*,[10-12] Wong,[20] Anderson *et al.*,[21,22] and more recently Nemirovsky *et al.*,[16-18] demonstrated the existence of two types of tunneling: trap-assisted and band-to-band, with distinctively different temperature dependencies.

Thermal-trap-assisted tunneling, its temperature and voltage dependencies, is modeled in this study on the basis of the following assumptions:

(1) The transition of electrons takes place by thermal excitation from the valence band to a Shockley-Read recombination center, and then via tunneling from the trapping center to the conduction band (see Appendix A).

(2) The dominant trap energy in the thermal-trap-assisted tunneling process, coincides with the Fermi level.

The dominant trap energy is calculated with

$$E_t = E_F = \frac{E_g}{2} + \frac{kT}{q}\ln\left(\frac{m_h^*}{m_e^*}\right)^{3/4} - \frac{kT}{q}\ln\left(\frac{N_A}{n_i}\right), \quad (1)$$

where N_A is the effective doping in the depletion region, E_g is the bandgap energy, and (m_h^*/m_e^*) is the ratio of the effective masses of holes and electrons. The Fermi energy is measured relative to the valence band.

The physical picture underlying the second assumption of this model is that there is a uniform distribution of trapping centers, throughout the bandgap and that the barrier for tunneling is lowest at the uppermost center that is still occupied. Hence, the occupied trapping center that coincides with the Fermi level, has the highest transition probability and plays the most dominant role in the thermal-trap-assisted tunneling process.

This assumption is responsible for the unique features of the model and explains the different temperature and bias dependencies of thermal-trap-assisted tunneling compared to band-to-band tunneling: tunneling currents that increase with increasing temperature and decreasing doping level and which exhibit ohmic-like regions and soft breakdown.

For modeling, we use the expression for the current density derived in Appendix A. The thermal-trap-assisted tunneling current density J_{TAT} is given by

$$J_{TAT} = qN_t\left(\frac{c_p p_1 wN_c}{c_p p_1 + wN_c}\right)x_D \,(\mathrm{A/cm^2}), \quad (2)$$

where N_t and c_p are the trap density and hole capture coefficient, respectively and x_D is the depletion region width.

Since the model assumes that $E_t = E_F$,

$$p_1 = N_v \exp(-E_F/kT), \quad (3)$$

and the tunneling rate is

$$wN_c = \frac{6\times10^5 E}{(E_g - E_F)} \times\exp\left[-\frac{1.7\times10^7 E_g^{1/2}(E_g - E_F)^{3/2}}{E}\right]\,[\mathrm{s}^{-1}], \quad (4)$$

where E is the electric field associated with the tunneling barrier (see Appendix A).

The dynamic resistance-arca product due to thermal-trap-assisted tunneling is given by

$$(\mathrm{RA})_{TAT} = \left(\frac{\partial J_{TAT}}{\partial V}\right)^{-1}, \quad (5)$$

and an analytic expression is derived in Appendix B. The following two limiting cases emerge.

(a) For $c_p p_1 \ll wN_c$, Eq. (2) reduces to

$$J_{TAT} \cong q(N_t c_p)p_1 x_D. \quad (6)$$

In this case, the tunneling rate is larger than the thermal transition rate, and the dark current is limited by the thermal transition. It should be noted that the thermal-assisted dark current in this limiting case of thermal-trap-assisted tunneling, can be significantly larger than the thermally limited generation current from the depletion region obtained by the normal Shockley-Read model, $J = q(n_i/2\tau_0)x_d$ as $p_1 \gg n_i$.

(b) For $c_p p_1 \gg wN_c$, Eq. (2) reduces to

$$J_{TAT} \cong qN_t(wN_c)x_D. \quad (7)$$

In this case, the tunneling rate is smaller than the thermal transition rate, and it determines the magnitude of the dark current.

In both cases, the dark current density is directly proportional to the density of trapping centers N_t. In the first case, limited by the thermal transitions, the dark current is directly proportional to the product of the density of trapping centers and the capture coefficient for holes, i.e. $N_t c_p$.

According to the model presented in this study, the tunneling rate wN_c exhibits the expected tunneling dependence for composition x and electric field E. It is easily seen from Eq. (4) that wN_c increases with increasing electric field and reduced composition and bandgap. However, wN_c exhibits an unexpected temperature and doping level dependence. With increasing temperature and decreasing doping level, the Fermi level and hence the dominant trap level is shifted to higher energies. Thus, the barrier for tunneling is reduced and wN_c increases, in contrast to direct band-to-band tunneling.

The magnitude of the tunneling rate wN_c as compared to the hole emission rate $c_p p_1$, determines the significance of the two limiting cases. At higher temperatures and electric fields, the limiting case (a) is obtained and the dark current can be approximated with Eq. (6). At lower temperatures and electric fields the limiting case (b) is obtained and the dark current can be approximated with Eq. (7).

To illustrate the unique features of this model thermal-trap-assisted tunneling is compared to direct band-to-band tunneling. Direct band-to-band tunneling is modeled with the simple approach of a triangular barrier determined by the bandgap.[10,28] The direct band-to-band tunneling current density J_{BTB} is given by[10]

$$J_{BTB} = 10^{-2}N_A^{1/2}V_t^{3/2}\exp\left[-\frac{3\times10^{10}E_g^2}{(N_A V_t)^{1/2}}\right]\,(\mathrm{A/cm^2}). \quad (8)$$

The RA product associated with direct band-to-band tunneling is given by

$$(\mathrm{RA})^{-1}_{\mathrm{BTB}} = 10^{-2} N_A^{1/2} \exp\left(\frac{-4\times10^{10}E_g^2}{(N_A V_t)^{1/2}}\right) \times\left(\frac{3}{2} V_t^{1/2} + \frac{3\times10^{10}E_g^2}{2N_A^{1/2}}\right). \quad (9)$$

The total dark tunneling current is calculated and modeled with

$$J = J_{\mathrm{BTB}} + J_{\mathrm{TAT}}. \quad (10)$$

The total dynamic resistance-area product is calculated and modeled with

$$\left(\frac{1}{\mathrm{RA}}\right)_{\mathrm{TOT}} = \left(\frac{1}{\mathrm{RA}}\right)_{\mathrm{BTB}} + \left(\frac{1}{\mathrm{RA}}\right)_{\mathrm{TAT}}. \quad (11)$$

The temperature dependence of the thermal-trap-assisted tunneling current density J_{TAT} is exhibited in Fig. 1. The unique features of thermal-trap-assisted tunneling become apparent by comparing it with the temperature dependence of direct band-to-band tunneling.

Figure 1(a) exhibits the remarkably different temperature dependencies of the two types of tunneling. Whereas direct band-to-band tunneling is reduced as temperature and hence bandgap increase, thermal-trap-assisted tunneling increases. This behavior results directly from the assumption $E_t \simeq E_F$.

Figure 1(b) exhibits the remarkably different dependencies on doping level of the two types of tunneling. Whereas direct band-to-band tunneling increases with doping level due to reduced barrier width, thermal-trap-assisted tunneling decreases with doping level. Again, this distinctive behavior results directly from the assumption $E_t \cong E_F$.

Figure 1(c) exhibits the temperature dependence of the two tunneling mechanisms with electric field as a parameter. Again, the remarkably different behavior of the two types of tunneling processes, become apparent. Direct band-to-band tunneling is very sensitive to the electric field whereas the dark current associated with thermal-trap-assisted tunneling is not sensitive to the higher electric fields. This stems from the fact that at high fields $wN_c \gg c_p p_1$ and the limiting case (a) prevails.

Figure 1(d) exhibits the effect of the trapping center density upon the dark current associated with thermal-trap-assisted tunneling. The dark current is directly proportional to the density of trapping centers. In the thermal-limited case, it is also directly proportional to the hole capture coefficient.

The bias dependence of the thermal-trap-assisted tunneling current density is exhibited in Fig. 2. This type of tunneling is characterized by current-voltage characteristics that at medium and high bias voltage exhibit nearly "Ohmic regions". The "Ohmic regions" occur for the thermally limited case (a) where the tunneling rate is larger than the capture rate. As we change the parameters that increase wN_c, the "Ohmic regions" are obtained at lower bias voltages. In Fig. 2(a) the "Ohmic region" is obtained at lower bias voltages as the temperature and hence wN_c is increased. Figure 2(b) and 2(c) exhibit the effect of trapping density and capture coefficient.

Figure 3 exhibits the transition from hard breakdown to soft breakdown as thermal-trap-assisted tunneling is includ-

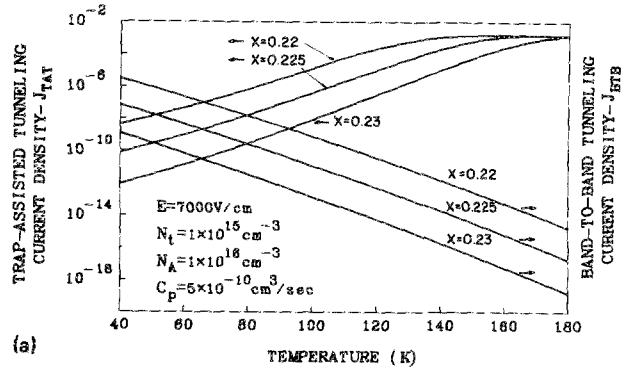

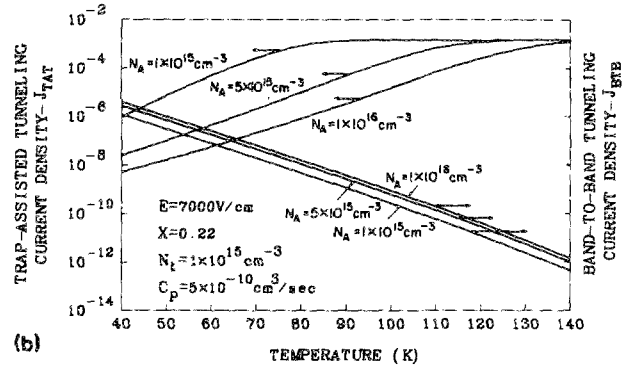

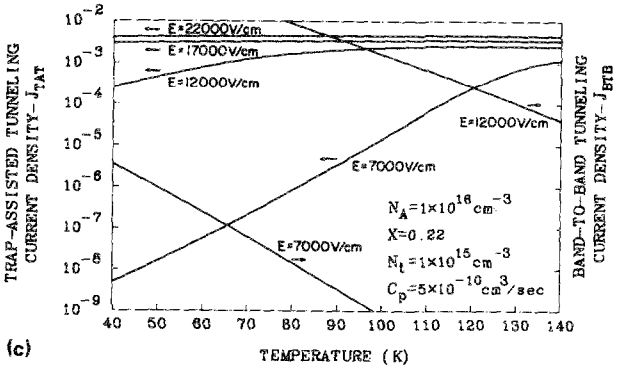

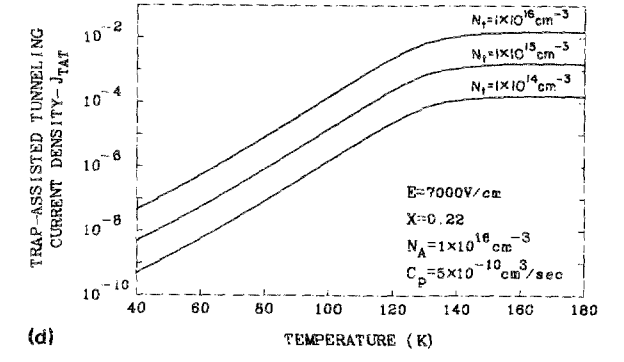

FIG. 1. Calculated thermal-trap-assisted tunneling current density J_{TAT} [Amp/cm^2] and band-to-band tunneling current density J_{BTB} [Amp/cm^2] versus temperature for $Hg_{1-x}Cd_xTe$. (a) with composition x as a parameter, (b) with doping level N_a [cm^{-3}] as a parameter, (c) with electric field E as a parameter, and (d) with density of trapping centers N_t [cm^{-3}] as a parameter. Note: The current scale is logarithmic.

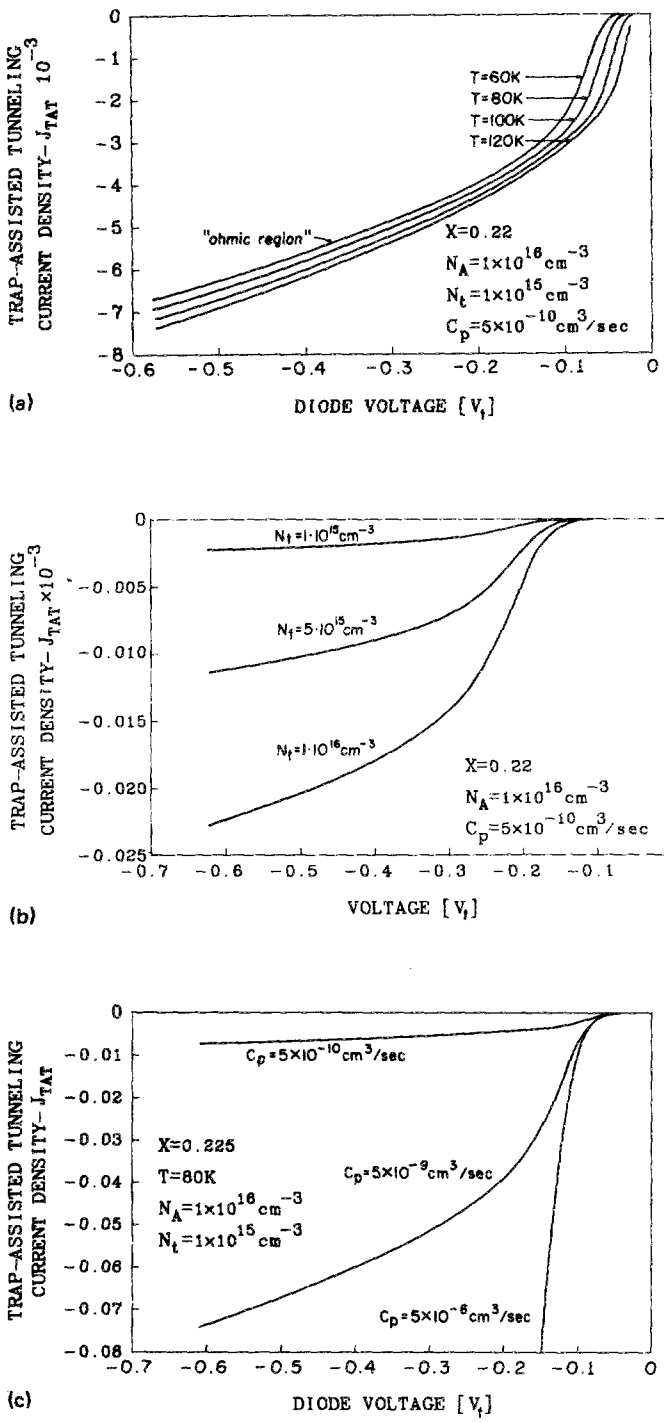

FIG. 2. Calculated thermal-trap-assisted tunneling current density J_{TAT} [Amp/cm^2] versus diode voltage for $Hg_{1-x}Cd_xTe$. (a) with temperature T as a parameter, (b) with density of trapping centers N_t [cm^{-3}] as a parameter, and (c) with capture coefficient of holes c_p [cm^{-3}] as a parameter. Note: The current scale is linear.

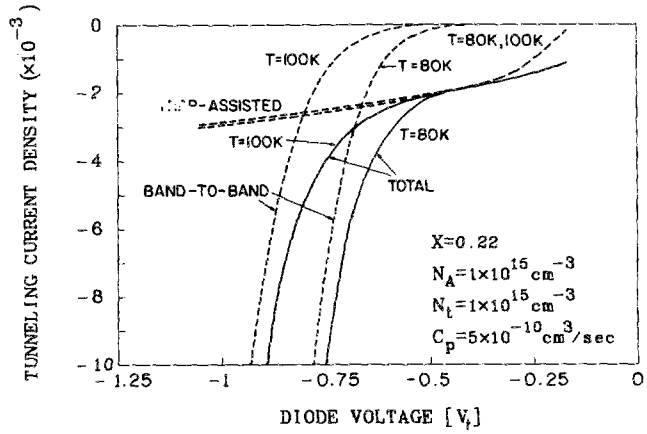

FIG. 3. A comparison of the calculated current-voltage characteristics of $Hg_{1-x}Cd_xTe$ diodes with $x = 0.22$ for trap-assisted tunneling and band-to-band tunneling (dashed lines). The total (combined) tunneling current-voltage characteristics are also shown (solid lines).

ed in the model. Direct band-to-band tunneling is characterized with hard breakdown behavior and the breakdown voltage is shifted to higher bias voltages as temperature increases. The "Ohmic region" exhibited by thermal-trap-assisted tunneling tends to soften the breakdown. This behavior has been observed empirically in numerous experiments (see for instance Fig. 5 in Ref. 16 and Fig. 3 in Ref. 13).

The calculated dependence of the dynamic resistance-area (RA) product of HgCdTe photodiodes as a function of reciprocal temperature, with the diode reverse-bias voltage as a parameter, is shown in Fig. 4. The total $(RA)_{TOT}$ product of Fig. 4(a) is calculated with Eq. (11) and the contribution of both types of tunneling—direct band-to-band and thermal-trap-assisted tunneling, is taken into account. The total $(RA)_{TOT}$ product exhibits a maximum around 60 K. Above approximately 60 K, as temperature increases, $(RA)_{TOT}$ decreases significantly. Below ~60 K, as temperature decreases, $(RA)_{TOT}$ decreases again but less sharply. Figure 4(b) exhibits the relative contribution of the two tunneling processes. The thermal-trap-assisted tunneling limited $(RA)_{TAT}$ product increases as temperature decreases whereas the direct band-to-band tunneling limited $(RA)_{BTB}$ product decreases as temperature is reduced. Hence, the resulting total $(RA)_{TOT}$ product exhibits a maximum. At higher temperatures for lower and medium reverse bias voltages, the total $(RA)_{TOT}$ product is limited by thermal-trap-assisted tunneling and at lower temperatures and higher reverse bias voltages, the total $(RA)_{TOT}$ product is limited by direct band-to-band tunneling.

The model presented in this study explains, for the first time, the observed maxima of the dynamic resistance $(RA)_{TOT}$ as a function of reciprocal temperature, as well as the overall measured temperature dependence of the (RA) product that was previously reported (for example, Fig. 7 of Ref. 16).

The relative contribution of the two tunneling processes determine the measured temperature dependence of the dynamic resistance. At low and medium reverse-bias regions, thermal-trap-assisted tunneling dominates, and the measured dynamic resistance $(RA)_{TOT}$ product increases as temperature is reduced. At lower temperatures and higher reverse-bias voltages, the contribution of band-to-band tunneling increases, and the associated $(RA)_{TOT}$ product de-

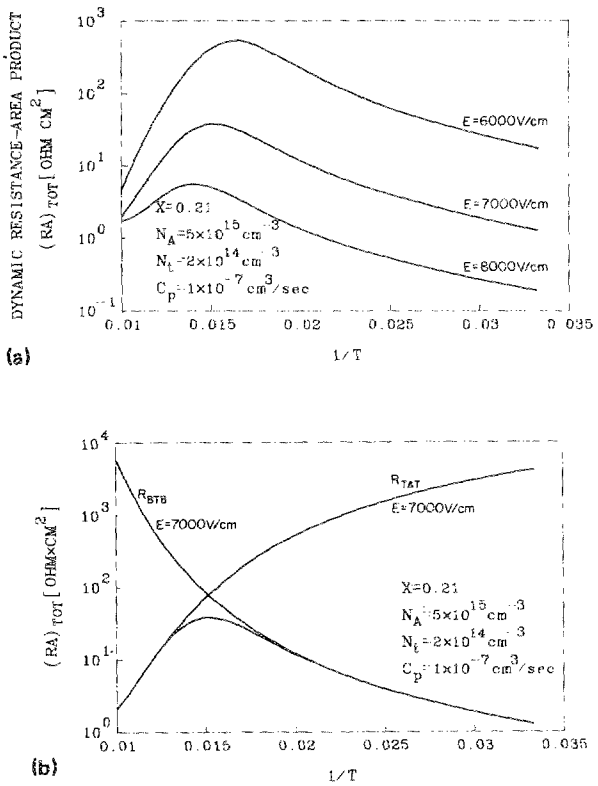

FIG. 4. (a) Dependence of the calculated total dynamic resistance of $Hg_{1-x}Cd_xTe$ $N+P$ diodes with $x=0.21$ upon reciprocal temperature with the maximum electric field at the junction as a parameter. (b) Dependence of the calculated trap-assisted tunneling and band-to-band dynamic resistance (dashed lines) and combined (total) dynamic resistance (solid line) upon reciprocal temperature. (c) Calculated dependence of the R_0A product upon reciprocal temperature.

creases. Hence, the measured $(RA)_{TOT}$ versus $1/T$, characteristics exhibit a maximum and either a plateau that is almost independent of the temperature or a decrease in the $(RA)_{TOT}$ at higher biases and lower temperature.

The model also accounts for the somewhat unexpected temperature dependence of the measured (R_0A) product at zero bias, at low temperatures. The measured diodes show a plateau in the R_0A value and a gradual increase toward lower temperatures.[13-22] Figure 4(c) exhibits the calculated thermal-trap-assisted tunneling limited resistance $(RA)_{TAT}$ at zero bias. The temperature dependence as well as the calculated values of the $(R_0A)_{TAT}$ product correspond to the typically measured data (e.g., Fig. 2 of Ref. 16).

It was previously observed that LWIR HgCdTe photodiodes exhibit (R_0A) product that become temperature insensitive with decreased temperature of operation and the values can vary by several orders of magnitude.[13-15] The values of the (R_0A) product of Fig. 4(c) as predicted by the model, are very sensitive to the density of traps, N_t and the capture coefficient c_p. Apparently, the trapping properties of state-of-the-art arrays fabricated on current materials, vary significantly.

The calculated dependence of the dynamic resistance-area $(RA)_{TOT}$ product as a function of diode reverse bias, is shown in Fig. 5. The thermal-trap-assisted tunneling limited $(RA)_{TAT}$ product is characterized by a nearly constant value at medium and high bias voltage. This behavior stems from the "Ohmic region" exhibited by the current–voltage characteristics. The direct band-to-band tunneling limited $(RA)_{BTB}$ product is characterized by a sharp fall as diode reverse-bias voltage increases. Typically, below 60 K the $(RA)_{TOT}$ product is limited by direct band-to-band tunnel-

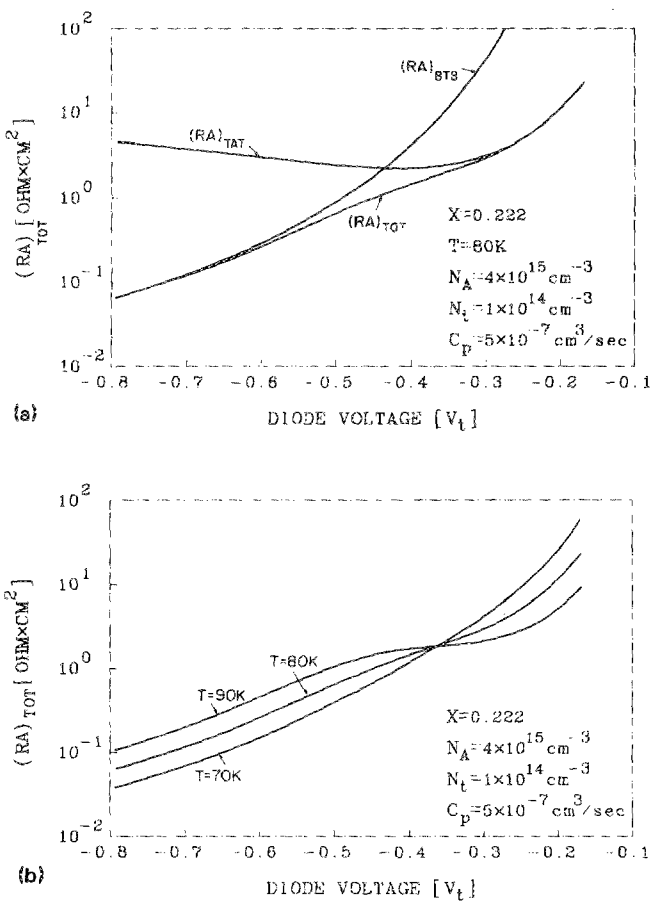

FIG. 5. Dependence of the calculated trap-assisted tunneling and band-to-band dynamic resistance (dashed lines) and combined (total) dynamic resistance (solid line) upon diode voltage. (a) At $T=80$ K, (b) Dependence of the total tunneling dynamic resistance upon diode voltage with the temperature T as a parameter.

ing whereas above 100 K the $(RA)_{TOT}$ product is limited by thermal-trap-assisted tunneling. At normal operation temperature of approximately 80 K, thermal-trap-assisted tunneling limits the $(RA)_{TOT}$ product at medium reverse-bias voltage and as the diode reverse bias voltage increases, a transition occurs and band-to-band tunneling limits the $(RA)_{TOT}$ product.

Figures 4 and 5 illustrate the predictions of the model. However, the exact shape and the (RA) values are strongly dependent on the parameters used for modeling. The relative contribution of the two tunneling processes depends strongly on the physical structure of the junction (n^+p^-p or n^+p for ion implanted junctions and n^-p for diffused junctions), vacancy or impurity doping, the doping level, and obviously the density and nature of the trapping centers. At this stage, we lack an independent direct method for characterizing the traps in HgCdTe and the trap parameters are determined by the best fit to the measured data.

III. TRAPPING AND THE EXCESS CARRIER LIFETIME

The excess carrier lifetime is, in general, an extremely sensitive indicator of material quality. This is especially true for *p*-type $Hg_{1-x}Cd_xTe$ ($x\sim0.22$) at 77 K, whose lifetime is limited by Shockley-Read recombination.[23-26] Although it has not yet been established that material with higher excess carrier lifetimes yield "superior" diodes, a number of experiments have shown that the connection between the excess carrier lifetime and the dark current is accurately described by the diffusion model, for n^+/p diodes at zero bias and at temperatures $\geqslant$77 K.[13,16,19] According to this model, the dark current produced by the diffusion of thermally generated minority carriers in the neutral *p*-region is proportional to $(\tau_n)^{1/2}$, so that a larger excess carrier lifetime results in a higher R_0A product.

The simple relationship between the lifetime and the dark current, however, ceases to be valid under reverse bias conditions, when the tunneling processes described in Sec. II are significant. In this case, the lifetime is not explicitly contained in the expression for the tunneling current, but is an implicit parameter which is determined by the characteristics of the trapping centers. The relationship between the lifetime and the dark current is further complicated by the different tunneling mechanisms, and is dependent on whether band-to-band or thermal trap-assisted tunneling dominates and on the rate limiting step for the thermal trap-assisted process. One consequence of this is that, unlike the case of zero bias, the excess carrier lifetime is not a fundamental parameter in determining reverse bias characteristics. Measurements of the excess carrier lifetime, however, remain a valuable technique for characterizing the trapping centers which cause the tunneling current.

The concentration and capture rates of the trapping centers, along with bandgap, temperature, and electric field in the depletion region, determine the magnitude of the dark current due to thermal trap-assisted tunneling. As the excess carrier lifetime is limited by Shockley–Read recombination, measurements of the lifetime can be used to estimate many of the relevant parameters of the trapping centers. At this preliminary stage in relating lifetime measurements to thermal trap assisted tunneling, two questions are particularly important; the first is whether lifetime measurements alone can be used to estimate the concentration and capture rates of the trapping centers; and the second is whether the trapping centers which are characterized by lifetime measurements are the same as those which cause the thermal trap-assisted tunneling current.

In interpreting lifetime data, it is important to make a distinction between the three commonly measured lifetimes; the excess minority carrier lifetime, τ_n, the excess majority carrier lifetime, τ_p, the transient lifetime, τ_t. Each of these time constants is associated with the recombination of electrons and holes, however, each refers to a different aspect of this process and, therefore, provides different information. In *p*-type $Hg_{0.78}Cd_{0.22}Te$ the transient and the majority carrier lifetimes may be as much as 25 times greater than the minority carrier lifetime due to the presence of trapping centers.[23-26]

The meanings of the relevant lifetimes are briefly reviewed in Appendix C. The first step in the recombination process is the capture of the minority carrier by a S-R center. This process occurs within a characteristic time of $(N_t c_n)^{-1}$, where N_t is the density of trapping centers, and c_n is the minority carrier capture rate of the center. This time constant is referred to as the excess minority carrier lifetime, τ_n. Ignoring carrier re-emission, the second step in the recombination process is the capture of a majority carrier by the filled center. This process occurs within a characteristic time of $(p_0 c_p)^{-1}$, where p_0 is the carrier concentration, and c_p is the majority carrier capture rate. The majority carrier lifetime is simply the total time that the hole remains in the valence band, and is given by $\tau_p = (N_t c_n)^{-1} + (p_0 c_p)^{-1}$. Thus it is seen that the excess majority carrier lifetime is always greater than or equal to the minority carrier lifetime. When trapping is significant (i.e. $\tau_{majority} \gg \tau_{minority}$), as is often found in *p*-type HgCdTe with $x\sim0.22$ and $p_0\sim10^{16}$ cm^3, the transient lifetime, τ_t, can be shown to be approximately equal to the majority carrier lifetime. The mathematical expressions for the minority, majority, and transient lifetimes are given in Appendix C, along with useful approximations for *p*-type $Hg_{0.78}Cd_{0.22}Te$.

Traps can essentially be described by the Shockley-Read (SR) recombination statistics. Trapping differs from recombination only in the relative values of the capture coefficients. If the capture coefficient for the minority carrier is many times larger than that for the majority carrier, then the SR center is called a "trap" rather than a "recombination center". In this case, the SR centers are not only "stepping stones" between the valence and conduction bands, but also trap electrons and the density of excess trapped electrons is significant.

Several experimental methods have been used for measuring the "lifetimes" of *p*-type HgCdTe. These techniques can be divided into transient and steady-state methods. A large difference between steady-state and transient lifetimes is an indication of trapping effects (see Appendix C).

The steady-state methods (including steady-state photoconductivity, zero bias resistance and diffusion length) yield

the excess minority carrier lifetime which to a good approximation is given by:

$$\tau_n \approx \frac{1}{c_n N_t}. \tag{12}$$

The transient methods (including photoconductive decay and diode reverse recovery) yield to a good approximation the majority carrier lifetime

$$\tau_t \approx \tau_p \approx \frac{1}{c_n N_t} + \frac{1}{c_p P_0}. \tag{13}$$

Independent measurement of the minority and majority carrier lifetimes (i.e. the steady-state and transient lifetimes) can be used to determine trap properties. However, Eqs. (12) and (13) include three unknown parameters: the density of traps, N_t, and the capture coefficients for minority and majority carriers c_n, c_p. Hence, additional information obtained by deep-level transient spectroscopy (DLTS)[1,3,4] is required.

Since the large difference between the steady-state minority carrier lifetime and the transient lifetime should occur due to the highly asymmetric capture coefficients, we assume

$$\frac{c_n}{c_p} \approx 10\text{–}10^2. \tag{14}$$

Trap properties determined by DLTS indicate that the capture coefficients are indeed highly asymmetric with the electron capture coefficient approximately two orders of magnitude larger than the hole capture coefficient.

Table I contains measured lifetimes (steady state and transient) for vacancy doped (undoped) material as well as impurity (Au or As) doped material. The corresponding traps properties are calculated with Eqs. (12)–(13).

$$c_p \approx \frac{1}{(\tau_t - \tau_n)p}, \tag{15}$$

$$c_n \approx 50 c_p, \tag{16}$$

and

$$N_t \approx \frac{1}{c_n \tau_n} \approx \left(\frac{c_p}{c_n}\right)\left(\frac{\tau_t - \tau_n}{\tau_n}\right) p_0. \tag{17}$$

Table I summarizes the results of 15 samples grown and doped by several methods, yet the derived capture coefficient for holes is almost the same for all the measured samples and is approximately 3×10^{-9} cm^3/s which is a reasonable value for the majority carrier capture coefficient and compares well to the DLTS data. The density of traps varies between 1×10^{14} cm^3 in the higher quality HgCdTe to $\sim6\times10^{15}$ cm^3 at the higher doped HgCdTe. This range of values is similar to that obtained by fitting the dc properties of measured photodiodes with the model described in Sec II.

Given the values of the majority carrier capture rates determined by lifetime measurements ($\sim10^{-10}$–10^{-9} cm^3/s), it is somewhat surprising that those used in the tunneling model in order to yield reasonable dark currents are at least two orders of magnitude larger ($\sim10^{-7}$ cm^3/s). Since the majority carrier capture rates determined by DLTS tend to be in the range of $10^{-11} - 10^{-10}$ cm^3/s, the discrepancy between DLTS measurements and the tunneling model is even greater. Besides the discrepancies in the absolute values of the capture rates, the type of trapping or recombination center is also in question. The large differences observed in the transient and minority carrier lifetimes indicate the recombination occurs at a donor-like trap. DLTS measurements also show that the traps are donor-like, for the material which has been characterized. However, the large value of the majority carrier capture rate needed in the tunneling model suggests that an acceptor-like center is responsible for the trap-assisted tunneling current. Other trap-assisted tunneling models have used similarly large values of the majority carrier capture rate in order to fit the data.[12]

At the present time, the discrepancy between the lifetime and DLTS data, and the trap-assisted tunneling parameters has not been resolved. One possible explanation is that the

TABLE I. Calculated traps properties from measured "lifetimes" in undoped and doped p-type HgCdTe from several sources.

Sample no.	Growth method	Dopant	Doping level at 77 K p_0(cm^{-3})	τ_n(ns)	τ_t(ns)	$c_p\times10^{9}$ [cm^3/s]	$c_n\times10^{-7}$ [cm^3/s]	Trap density N_t[cm^{-3}]
SAT86	THM	None	3.5×10^{15}	28	100	4	2	1.4×10^{14}
N628	SSR	None	6.8×10^{15}	11	72	2.4	1.2	7.5×10^{14}
862-7	SSR	None	8.9×10^{15}	2.7	35	3.5	1.7	2.1×10^{14}
P1637	Slush	None	1.5×10^{16}	1.4	23	3.1	1.5	4.7×10^{15}
THM6-36	THM	None	4.4×10^{15}	10	23	3.1	1.5	4.7×10^{14}
855-1	SSR	None	9.0×10^{15}	8	36	4	2	6×10^{15}
861-3	SSR	As	1.2×10^{16}	62	90	3	1.5	1×10^{14}
850-3	SSR	As	1.6×10^{16}	11	40	2	1	8.4×10^{14}
ND74-A1	SSR	As	5.6×10^{15}	47	115	2.6	1.3	1.6×10^{14}
860-1	SSR	As	1.1×10^{16}	2.5	38	2.5	1.3	3.1×10^{15}
867-1	SSR	As	6.1×10^{15}	8	90	2	1	1.2×10^{15}
809-1	SSR	Au	6.2×10^{15}	49	220	0.9	0.5	4.3×10^{14}
716-3-6	SSR	Au	7.0×10^{15}	10	80	2	1	1×10^{15}
818-1	SSR	Au	8.3×10^{15}	1.6	50	2.5	1.2	5×10^{15}
835-3	SSR	Au	8.3×10^{15}	6.0	62	2.8	1.4	5×10^{15}

centers which limit the lifetime are different than those which contribute to the tunneling current. In addition, it should be noted that the measured lifetimes of Table II characterize the traps in the neutral *p*-type region of the substrate, while thermal-trap-assisted tunneling dark currents are generated at the depletion region. Hence, the relevant traps for this mechanism physically reside at the junction and it is highly probable that the nature and the properties of these traps are determined by the junction formation technology. A second possible explanation is that the value used for the matrix element of the trap potential (see Appendix A) is too small, resulting in an underestimation of the tunneling current.

IV. SUMMARY

Comprehensive experimental studies of HgCdTe ($x \cong 0.22$) MIS and junction photodiodes, fabricated by alternative junction formation technologies, utilizing different substrates and different passivation techniques, have one common feature; they indicate that traps and trap-assisted processes play a dominant role in limiting device performance and contributing large nonuniformities along arrays.

Trap-assisted tunneling has previously been proposed as a dominant mechanism contributing a significant component to dark currents and noise currents, over a wide range of operating temperatures and bias voltages.[10–22] The mechanism associated with trap-assisted tunneling was identified and characterized with a positive temperature coefficient. In addition, it was observed that the physical processes associated with trap-assisted tunneling contributed an Ohmic current component in the so-called reverse bias saturation region at relatively high temperatures with an empirical temperature dependence that follows $\exp \gamma T$. The same mechanism also limited the zero bias dynamic resistance R_0 at lower temperatures.[13–15]

However, the observed temperature and voltage dependence and behavior of trap-assisted tunneling remained unexplained, and the role of traps in limiting device performance could not be taken into account quantitatively.

In this paper, we model the trap-to-band process that limits the performance of LWIR HgCdTe diodes (junction as well as MIS structures). We analyze thermal-trap-assisted tunneling where the transition of electrons takes place by thermal excitation from the valence band to a Shockley–Read recombination center, and then via tunneling from the trapping center to the conduction band.

This combined mechanism was considered and studied in the past.[10–12] However, it was previously assumed that even though there are probably a large number of SR levels through the band gap, the trap-assisted tunnel current should be dominated by traps located somewhere near the middle of the gap where tunnel transitions from the valence and conduction bands are approximately equal.

In our study, we propose a significantly different assumption, i.e., that the dominant trap energy coincides with the Fermi level. Indeed, there is most probably a distribution of S-R levels throughout the band gap. However, the traps adjacent to the Fermi level are characterized by a high probability of occupation and a high transition probability, since the tunneling barrier is relatively low.

The combined process of thermal-trap-assisted tunneling together with the assumption that the dominant trap coincides with the Fermi level, are modeled in this paper to yield the correct temperature and bias dependence (i.e. the positive temperature coefficient, the Ohmic behavior and the soft breakdown that have been experimentally observed). The experimental observations and the associated models emphasize that state-of-the-art photodiodes are limited by thermal-trap-assisted tunneling at low and medium reverse bias regions at higher temperatures of operation, and a combination of band-to-band tunneling and thermal-trap-assisted tunneling at lower temperatures and higher reverse-bias voltages. These observations illuminate the highly significant role of material properties in the overall performance of detectors.

The experiments and modeling indicate that control of traps is a key problem in the program for high-performance infrared focal plane arrays. Control of doping, electrical field profiles and barrier heights associated with control of band gap, trap density, and capture coefficients, become inter-related and stringent because the tunneling probability factors (band to band as well as thermal trap assisted) contain these parameters in an exponential.

Progress in the elucidation and characterization of traps and trapping effects in Hg CdTe is required, if we are to set to improve the performance of state-of-the-art arrays. The role of traps and trapping effects should be addressed by the modern and advanced epitaxial growth methods.

APPENDIX A

The major mechanism of thermal-trap-assisted tunneling (TAT) in MIS and n^+p HgCdTe photodiodes is assumed to include thermal excitation from the valence band to a Shockley–Read recombination and trapping center N_t, and then tunneling from the center to the conduction band.

The net capture rate of electrons into N_t centers is

$$U_n = c_n n(N_t - n_t) - c_n n_1 n_t - n_t w(N_c - n_c) + (N_t - n_t) w n_c, \quad \text{(A1)}$$

where N_t is the density of trapping centers, n_t is the density of N_t centers occupied by electrons, n_c is the density of electrons in the conduction band at the tunneling energy, c_n is the capture coefficient for electrons, N_c is the density of states in the conduction band, w is the tunneling probability from the N_t center to the conduction band, and $n_1 = N_c \exp[-(E_g - E_t)/kT]$, and E_t is the trap energy measured from the valence band.

The first two terms in Eq. (A1) describe the normal Shockley–Read thermal generation-recombination processes and the third and fourth terms describe the tunneling transitions between the trapping center and the conduction band.

The net capture rate of holes is given by the Shockley-Read theory

$$U_p = c_p p n_t - c_p p_1 (N_t - n_t), \quad \text{(A2)}$$

where c_p is the capture coefficient for holes, $p_1 = N_v \exp[-E_t/kT]$, and N_v is the density of states in the valence band.

In steady-state, $U_n = U_p$, giving the function of occupied centers

$$\frac{n_t}{N_t} = \frac{c_n n + c_p p_1 + w n_c}{c_p(p + p_1) + c_n(n + n_1) + w N_c}. \tag{A3}$$

By combining Eqs. (A1)–(A3), the net combination rate which is determined by the density of trapping centers, their capture properties, tunneling rate, and doping level, is obtained:

$$U = U_n = U_p = N_t \frac{c_p c_n (np - n_i^2) + c_p w[n_c p - p_1(N_c - n_c)]}{c_p(p + p_1) + c_n(n + n_1) + w N_c}. \tag{A4}$$

For depletion regions where $n \approx 0, p \approx 0$,

$$U = N_t \frac{-c_p c_n n_i^2 - c_p p_1 (N_c - n_c) w}{c_p p_1 + c_n n_1 + w N_c}. \tag{A5}$$

Equation (A5) is further simplified by assuming that the dominant transition between the trapping centers and the conduction band is via tunneling and $c_n n_1 \ll w N_c$. In addition $N_c \gg n_c$ and $c_p p_1 w N_c \gg c_p c_n n_i^2$. Hence,

$$U = -N_t \frac{c_p p_1 w N_c}{c_p p_1 + w N_c}. \tag{A6}$$

The expression for the dark current density due to trap-assisted tunneling is

$$J_{\mathrm{TAT}} = qN_t \left[\frac{c_p p_1 w N_c}{c_p p_1 + w N_c}\right] x_d \quad [\mathrm{A/cm^2}], \tag{A7}$$

where x_d is the width of the depletion layer.

The thermal-trap-assisted tunneling current density of Eq. (A7) describes thermal transitions of electrons from the valence band into trapping centers and subsequently tunneling transitions of electrons from the trapping centers into the conduction band. Thermal transitions from the trapping centers into the conduction band are neglected as well as the tunneling transitions into the trapping centers from the valence band.

The thermal transition rate (e_n) from mid-band-gap traps into the conduction band is much lower than the corresponding thermal transition rate to the valence band (e_p) due to the low density of states associated with the conduction band ($e_n = c_n n_1 \sim c_n N_c$)

The tunneling rate of electrons from the valence band into the traps is much lower than band-to-band tunneling from the valence band into the conduction band, since the barrier for tunneling is nearly the same (E_g) and the density of states in the conduction band is higher than the density of traps.

Following Sah[29] and Kinch,[10] the tunneling rate is given by

$$w N_c = \frac{\pi^2 q m_e^* E M^2}{h^3 (E_g - E_t)} \exp\left[-\frac{4(2m_e^*)^{1/2}(E_g - E_t)^{3/2}}{3hqE}\right], \tag{A8}$$

where M is the matrix element of trap potential, m_e^* is the effective mass of electrons, and E is the electric field associated with the tunneling barrier.

The experimentally determined value of $[M^2(m_e^*/m)]$ for silicon is 10^{-23} V cm^3 and is adopted for the HgCdTe calculations. Hence,

$$w N_c = \frac{6\times 10^5 E}{(E_g - E_t)} \exp\left[\frac{-1.7\times 10^7 E_g^{1/2}(E_g - E_t)^{3/2}}{E}\right], \tag{A9}$$

where E_g and $(E_g - E_t)$ are in volts, and E in V/cm.

APPENDIX B

The dynamic resistance-area product due to thermal-trap-assisted tunneling is derived with:

$$(\mathrm{RA})_{\mathrm{TAT}}^{-1} = \frac{\partial J_{\mathrm{TAT}}}{\partial w N_c} \cdot \frac{\partial w N_c}{\partial E} \cdot \frac{\partial E}{\partial V} \tag{B1}$$

where J_{TAT}, wN_c are given by Eqs. (2) and (3), respectively. E is the electric field and is given by $E = (qN_A/\epsilon_0\epsilon_s)^{1/2}(2V_t)^{1/2}$. Hence,

$$\frac{\partial J_{\mathrm{TAT}}}{\partial w N_c} = \frac{(c_p P_1 + w N_c)\cdot q N_t c_p P_1 - q N_c c_p P_1 w N_c}{(c_p P_1 + w N_c)^2} = \frac{q N_t \cdot (c_p P_1)^2}{(c_p P_1 + w N_c)^2}, \tag{B2}$$

$$\frac{\partial w N_c}{\partial E} = \frac{6\times 10^5}{(E_g - E_t)} \exp\left(-\frac{1.7\times 10^7 \cdot E_g^{1/2}(E_g - E_t)^{3/2}}{E}\right) \times \left(1 + \frac{1.7\times 10^7 \cdot E_g^{1/2}\cdot (E_g - E_t)^{3/2}}{E}\right) = \frac{w N_c}{E} \cdot \left(1 + \frac{1.7\times 10^7 \cdot E_g^{1/2}\cdot (E_g - E_t)^{3/2}}{E}\right), \tag{B3}$$

$$\frac{\partial E}{\partial V} = \sqrt{qN_a/2\epsilon_0\epsilon_s V_t} \tag{B4}$$

$$\frac{1}{(\mathrm{RA})_{\mathrm{TAT}}} = \frac{q\cdot N_t (c_p P_1)^2}{(c_p P_1 + w N_c)^2} \cdot \frac{w N_c}{E} \times \left(1 + \frac{1.7\times 10^7 \cdot E_g^{1/2}\cdot (E_g - E_t)^{3/2}}{E}\right) \times \left(\frac{qN_A}{2\epsilon_s\epsilon_0 V}\right)^{1/2}. \tag{B5}$$

By combining Eqs. (B1)–(B5) we obtain

$$\frac{1}{(RA)_{TAT}} = \left\{ qN_t (C_p P_1)^2 \cdot \frac{6\times 10^5}{(E_g - E_t)} \exp\left[- \frac{1.7\times 10^7 \cdot E_g^{1/2} \cdot (E_g - E_t)^{3/2} (\epsilon_s \epsilon_0)^{1/2}}{(2qN_A V)^{1/2}} \right] \right\}$$
$$\left(C_p P_1 + \left\{ \frac{6\times 10^5 (2qN_A V)^{1/2}}{(E_g - E_t)(\epsilon_s \epsilon_0)^{1/2}} \exp\left[\frac{1.7\times 10^7 \cdot E_g^{1/2} \cdot (E_g - E_t)^{3/2} (\epsilon_s \epsilon_0)^{1/2}}{(2qN_A V)^{1/2}} \right] \right\} \right)$$
$$\times \left[\frac{1.7\times 10^7 \cdot E_g^{1/2} \cdot (E_g - E_t)^{3/2} (\epsilon_s \epsilon_0)^{1/2}}{(2qN_A V)^{1/2}} \right] \left(\frac{qN_A}{2\epsilon_s \epsilon_0 V} \right)^{1/2}. \quad \text{(B6)}$$

APPENDIX C

The three lifetimes which are relevant to the characterization of p-type $Hg_{1-x}Cd_xTe$ are the excess minority carrier lifetime, τ_n, the excess majority carrier lifetime, τ_p, and the transient lifetime, τ_t. The particular lifetime which is measured depends on the experimental technique. The mathematical expressions for these lifetimes are given below, and differ depending on the amount of minority carrier trapping. According to the Shockley–Read theory, the steady state excess minority and majority carrier lifetimes are given by

$$\tau_n = \frac{\tau_{p0}(n_0 + n_1) + \tau_{n0}\{p_0 + p_1 + N_t[1 + (p_0/p_1)]^{-1}\}}{n_0 + p_0 + N_t[1 + (p_0/p_1)]^{-1}[1 + (p_1/p_0)]^{-1}} \quad \text{(C1)}$$

and,

$$\tau_p = \frac{\tau_{n0}(p_0 + p_1) + \tau_{p0}\{n_0 + n_1 + N_t[1 + (n_0/n_1)]^{-1}\}}{n_0 + p_0 + N_t[1 + (n_0/n_1)]^{-1}[1 + (n_1/n_0)]^{-1}}. \quad \text{(C2)}$$

According to Sandiford, the transient lifetime, which is the time constant describing the decay of excess carriers is given by:[30]

$$\tau_t = \frac{\tau_{n0}\{p_0 + p_1 + N_t[1 + (p_0/p_1)]^{-1}\} + \tau_{p0}\{n_0 + n_1 + N_t[1 + (n_0/n_1)]^{-1}\}}{n_0 + p_0 + N_t[1 + (n_0/n_1)]^{-1}[1 + (n_1/n_0)]^{-1}}, \quad \text{(C3)}$$

where $\tau_{n0} = (N_t \cdot c_n)^{-1}$, $\tau_{p0} = (N_t \cdot c_p)^{-1}$, N_t = density of trapping centers,

$$n_1 = N_c \cdot \exp(E_t - E_c)/kT,$$
$$p_1 = N_v \cdot \exp(E_v - E_t)/kT.$$

For p-type $Hg_{0.78}Cd_{0.22}Te$ at 77 K the relationship $p_0 \gg N_t \gg p_1$, $n_1 \gg n_0$, is usually valid, so we can simplify the above lifetime expressions to:

excess minority carrier lifetime:

$$\tau_n \approx \tau_{n0} = \frac{1}{N_t \cdot c_n}; \quad \text{(C4)}$$

excess majority carrier lifetime:

$$\tau_p \approx \frac{1}{N_t \cdot c_n} + \frac{1}{c_p \cdot p_0}; \quad \text{(C5)}$$

transient lifetime:

$$\tau_t \approx \frac{1}{N_t \cdot c_n} + \frac{1}{c_p \cdot p_0}. \quad \text{(C6)}$$

The following discussion briefly reviews the several time constants which characterize the recombination and trapping processes and are known as the "lifetimes."[26]

The excess electron lifetime, τ_n is defined by

$$U_n = \frac{\Delta n}{\tau_n} = c_n[n(N_t - n_t) - n_1 n_t], \quad \text{(C7)}$$

where U_n is the net recombination rate for electrons.

The first step in the SR recombination process is the capture of the minority carrier by a center. This process occurs within a characteristic time of $1/c_n N_t$ where N_t is the density of trapping centers, and c_n is the minority carrier capture coefficient of the center. This time constant is to a good approximation a measure of the excess electron lifetime. Thus,

$$\tau_n \approx \frac{1}{c_n N_t}. \quad \text{(C8)}$$

Accordingly, the excess hole lifetime, τ_p, is defined by

$$U_p = \frac{\Delta p}{\tau_p} = c_p[pn_1 - p_1(N_t - n_t)], \quad \text{(C9)}$$

where U_p is the net recombination rate for holes.

Under steady-state conditions

$$U_n = U_p, \quad \text{(C10)}$$

and hence,

$$\frac{\Delta n}{\tau_n} = \frac{\Delta p}{\tau_p}. \quad \text{(C11)}$$

It is usually assumed that $\Delta n \approx \Delta p$ and in this case, under steady-state conditions, the common recombination rate is related to the common excess carrier lifetime and

$$\tau_n = \tau_p \approx \frac{1}{c_n N_t}\left(1 + \frac{p_1}{p_0}\right). \quad \text{(C12)}$$

In the case of SR recombination involving trapping centers, space charge neutrality includes the trapped electrons and hence,

$$\Delta n + \Delta n_t = \Delta p, \tag{C13}$$

where Δn, Δn_t, and Δp are the excess electrons, trapped electrons and holes, respectively.

Thus, if trapping centers are present in the p-type material, $\Delta n < \Delta p$, and the electron and hole lifetimes will be different with $\tau_p > \tau_n$.

The excess trapped electrons are calculated with

$$\Delta n_t = N_t(f - f_0), \tag{C14}$$

where f and f_0 are the occupation factor of the centers in terms of electron and hole concentration, under steady-state and equilibrium, respectively. Hence,

$$\Delta n_t \approx \left(\frac{c_n N_t}{c_p p_0}\right) \Delta n. \tag{C15}$$

The density of trapped electrons and trapping effects become significant, if either $N_t \gg p_0$ or $c_n \gg c_p$.

With trapping, $\Delta n \neq \Delta p$ and the majority carrier lifetime becomes longer than the minority carrier lifetime. Equations (C11), (C13), and (C15) yield

$$\tau_p = \tau_n \left(\frac{\Delta p}{\Delta n}\right) = \tau_n \left(1 + \frac{\Delta n_t}{\Delta n}\right), \tag{C16}$$

and the majority carrier lifetime is

$$\tau_p \approx \frac{1}{c_n N_t} + \frac{1}{c_p p_0}. \tag{C17}$$

Thus, it is seen that the majority carrier lifetime is simply the time needed to capture a minority carrier ($1/c_n N_t$) plus the time needed for an occupied center to capture a majority carrier ($1/c_p p_0$).

In transient photoconductive decay, basically two time constants are measured and defined as the "lifetimes". These time constants are obtained by solving the three rate equations for electrons, holes and trapped electrons, with appropriate initial and final conditions.

Because of the electroneutrality condition, there are only two independent equations for the case of one trapping level, and hence, two time constants or "lifetimes" completely define the transient decay (τ_i,τ_t). To a good approximation,

$$\tau_i \approx \frac{1}{c_n N_t} \approx \tau_n, \tag{C18}$$

$$\tau_t \approx \frac{1}{c_n N_t} + \frac{1}{c_p p_0} \approx \tau_p. \tag{C19}$$

Thus, the two time constants characterizing the transient decay are approximately given by the steady-state minority and majority excess carrier lifetimes. These two lifetimes are different only if trapping effects are significant.

Experimental techniques that measure under steady-state conditions yield τ_n; transient techniques yield τ_t. A large difference between transient and steady-state lifetimes, is an indication of a considerable trapping effect.

[1] C. E. Jones, V. Noir, D. L. Polla, Appl. Phys. Lett. **39**, 248 (1981).
[2] D. Polla, S. G. Tobin, M. B. Reine, and A. K. Sood, J. Appl. Phys. **52**, 5182 (1981).
[3] C. E. Jones, V. Nair, J. Lindquestand and D. L. Polla, J. Vac. Sci. Technol. **21**, 1987 (1982).
[4] D. L. Polla, C. G. Jones, J. Appl. Phys. **52**, 5118 (1981).
[5] C. L. Littler, and D. G. Seiler, and M. R. Loloee, J. Vac. Sci. Technol. A **8**, 1133 (1990).
[6] D. T. Cheung, J. Vac. Sci. Technol. A **3**, 128 (1985).
[7] C. E. Jones *et al.*, J. Vac. Sci. Technol. A **3**, 128 (1985).
[8] C. W. Myles, J. Vac. Sci. Technol. A **6**, 2675 (1988).
[9] S. Goetting and C. G. Morgan-Pond, J. Vac. Sci. Technol. A **6**, 2675 (1988).
[10] M. A. Kinch, in *Semiconductors and Semimetals*, edited by R. K. Willardson and A. C. Beer, (Academic, New York, 1981), Vol. 18, p. 336.
[11] M. A. Kinch, J. Vac. Sci. Technol. **21**, 172 (1982).
[12] D. K. Blanks, J. D. Beck, M. A. Kinch, and L. Colombi, J. Vac. Sci. Technol. A **6**, 2790 (1988).
[13] R. E. DeWames, J. G. Pasko, E. Siyao, A. H. B. Vanderwyck, and G. M. Williams, J. Vac. Sci. Technol. A **6**, 2655 (1988).
[14] R. E. DeWames, G. M. Williams, J. G. Pasko, and A. H. B. Vanderwyck, J. Cryst. Growth **86**, 849 (1988).
[15] R. E. DeWames, *Tunneling in Small Band Gap HgCdTe P-N Junction* (Publisher, city 1989), page no.
[16] Y. Nemirovsky, D. Rosenfeld, R. Adar, and A. Kornfeld, J. Vac. Sci. Technol. A **7**, 528 (1989).
[17] Y. Nemirovsky, R. Adar, A. Kornfeld, and I. Kidron, J. Vac. Sci. Technol. A **4**, 1986 (1986).
[18] Y. Nemirovsky and D. Rosenfeld, J. Vac. Sci. Technol. A **8**, 1159 (1990).
[19] M. Reine, A. K. Sood, and T. J. Fredwell, in Semi-Conductors and Semimetals edited by R. K. Willardson and A. C. Beer (Academic, New York, 1981) Vol. 18.
[20] J. Y. Wong, IEEE Trans. Electron Devices, **ED-27**, 48 (1980).
[21] W. W. Anderson and H. J. Hoffman, J. Appl. Phys. **53**, 9130 (1982).
[22] W. W. Anderson and H. J. Hoffman, J. Vac. Sci. Technol. A **1**, 1730 (1983).
[23] R. Fastow and Y. Nemirovsky, Appl. Phys. Lett. **55**, 1982 (1989).
[24] R. Fastow and Y. Nemirovsky, J. Appl. Phys. **66**, 1705 (1989).
[25] R. Fastow and Y. Nemirovsky, J. Vac. Sci. Technol. A **8**, 1245 (1990).
[26] R. Fastow, D. Goren, and Y. Nemirovsky, J. Appl. Phys. **68**, 3405 (1990).
[27] A. van der Ziel, *Noise in Solid State Devices and Circuits* (Wiley, New York, 1986).
[28] S. M. Sze, *Physics of Semiconductor Devices* (Wiley Interscience, New York, 1982).
[29] C. T. Sah, Phys. Rev. **123**, 1594 (1961).
[30] D. J. Sandiford, Phys. Rev. **105**, 524 (1957).